Chapter 11

Topological Semimetals

*Short summary for online

In a lattice model for a d dimensional topological insulator, transitions between topological and trivial regimes can be induced by tuning some parameter λ. We can promote this parameter to a momentum, and thus obtain a $d+1$ dimensional lattice model. This is will be a topological semimetal, also called 0-gap insulator, where the bands touch at separated points. The band touching points are called Weyl nodes, they carry a topological charge, and therefore are topologically protected: continuous changes of parameters can move them, but cannot open a gap. To transition to an insulator, all Weyl nodes have to fuse with other nodes with opposite charge. Topological semimetals also have surface states, whose density depends on the orientation of the surface with respect to the crystallographic axis.

11.1 Coupling SSH Chains for a Two-dimensional Weak Topological Insulator

We construct a two-dimensional chiral symmetric lattice model by connecting several SSH chains to each other through nearest-neighbor hopping. The interchain hopping amplitudes w_y connect sites on opposite sublattices, so chiral symmetry is respected. As shown in Fig. 11.1, we obtain a so-called brick-wall lattice, rotated by 45 degrees.

The corresponding bulk momentum-space Hamiltonian reads,

$$H_{\mathrm{C2D}}(k) = \begin{pmatrix} 0 & v + w_x e^{-ik_x} + w_y e^{-ik_y} \\ v + w_x e^{ik_x} + w_y e^{ik_y} & 0 \end{pmatrix}. \tag{11.1}$$

Here we used v for the intracell hopping amplitudes, and w_x for the hopping along the chains. Expressed in terms of the Pauli matrices, this reads,

$$\hat{H}_{\mathrm{C2D}}(k) = (v + w_x \cos k_x + w_y \cos k_y)\hat{\sigma}_x + (w_x \sin k_x + w_y \sin k_y)\hat{\sigma}_y. \tag{11.2}$$

The system has chiral symmetry, inherited from the SSH chains, because of the

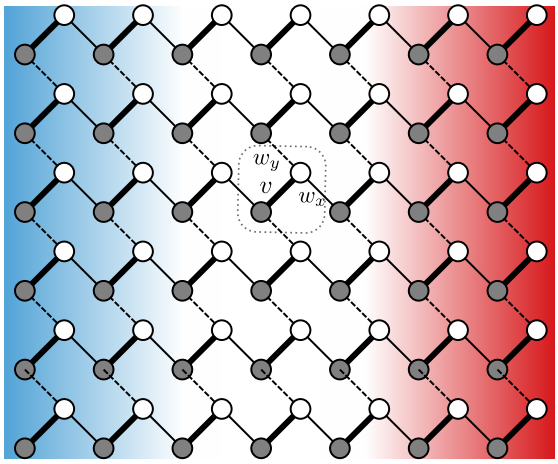

Figure 11.1: Geometry of the model. Filled (empty) circles are sites on sublattice A (B), each hosting a single state. They are grouped into unit cells, one of which is indicated by a dotted line. The intracell hopping amplitudes v are shown in thick lines, the intercell hopping amplitudes along the x and y axes, w_x and w_y, are shown is thin and dashed lines. The left and right edge regions are indicated by blue and red shaded background.

way we introduced with the interchain hoppings.

$$\text{Chiral symmetry} : \qquad \hat{\sigma}_z \hat{H}_{\text{C2D}}(k) \hat{\sigma}_z = -\hat{H}_{\text{C2D}}(k). \tag{11.3}$$

It also has inversion symmetry and time-reversal symmetry,

$$\text{Inversion symmetry} : \qquad \hat{\sigma}_x \hat{H}_{\text{C2D}}(k) \hat{\sigma}_x = \hat{H}_{\text{C2D}}(-k); \tag{11.4}$$

$$\text{Time-reversal symmetry} : \qquad \hat{H}_{\text{C2D}}(k) = \hat{H}^*_{\text{C2D}}(-k). \tag{11.5}$$

For the properties we focus on now, the symmetries besides chiral symmetry are not important. They can be broken, e.g., by making the intracell hopping complex, which modifies Eq. (11.2) by an extra term $\text{Im}(v)\hat{\sigma}_y$.

11.1.1 Weak Topological Insulator

We expect interesting physics if the two-dimensional model is composed of topological SSH chains ($w_x > v$) that are weakly coupled, $w_y \ll w_x, v$. We then have what is called a *weak topological insulator*: a two-dimensional insulator with a weak topological invariant, the k_y-independent winding number along the k_x axis.

A weak topological insulator has protected edge states, as can be understood by treating the interchain hopping w_y as a perturbation. These edge states can be seen on a numerical example shown in Fig. 11.2. Consider a straight boundary at some angle α with the x axis. For $w_y = 0$, we have a zero-energy eigenstate for each chain that

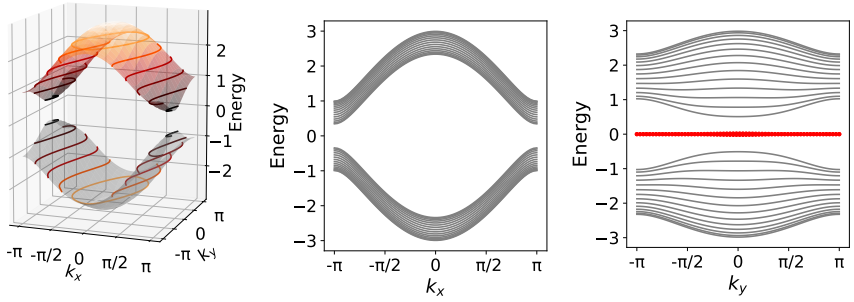

Figure 11.2: Dispersion relation of a weak topological insulator, obtained by coupling topological SSH chains ($v = 1$, $w_x = 5/3$), with interchain hopping $w_y = 1/3$. Left: bulk bands. Middle and Right: dispersion relations at an edge along x and y. Large (red) dots indicate edge states (whose wavefunction has over 40% weight within the first 4 unit cells of the total of 15 unit cells). These edge states only show up for a cut along y.

ends at the boundary, all of them on sublattice A (B). The linear density of these zero energy states is $\sin\alpha$. When we turn on the interchain hopping w_y, the energy of these states is topologically protected in the same way as for a single SSH chain: To move away from zero energy, they would need partners on the other sublattice, but no partner is available this side of the bulk. Although the edge states are at zero energy, they are nondispersive, and hence do not take part in conduction.

11.2 Transition from Trivial to Weak Topological Insulator is Broadened: Topological Semimetal

Consider how the two-dimensional chiral symmetric model can be tuned using the intercell hopping along the chains, w_x, from topologically trivial to a weak topological insulator. In the case of no interchain hopping, $w_y = 0$, we have a trivial insulator with $w_x < v$, and a weak topological one with $w_x > v$. There is a sudden transition from trivial to weak topological insulator at $w_x = v$, when the gap closes at $k_x = \pi$, which corresponds to a line spanning the two-dimensional Brillouin zone. We will see that in the presence of an interchain hopping w_y, this transition is broadened. The gap closes only at isolated momenta, the so-called nodes, which traverse the Brillouin zone as the control parameter drives the system through the transition.

To build on our understanding of the topology in the SSH model, we can demote k_y to a parameter, much in the same way as we did when we connected the Qi-Wu-Zhang model to the Thouless charge pump. Looking at the bulk Hamiltonian in this way, we have a continuous set of SSH models, with complex intracell hopping parameter $v_{\mathrm{SSH}}(k_y) = v + w_y \cos k_y + i w_y \sin k_y$, and intercell hopping $w_{\mathrm{SSH}}(k_y) = w_x$. The corre-

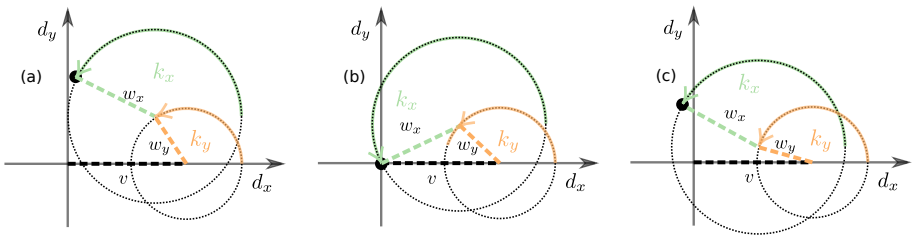

Figure 11.3: The curve on the $d_x - d_y$ plane, traced by the bulk Hamiltonian $\hat{H}_{\mathrm{C2D}}(k_x,k_y)$, at a fixed k_y, as k_x is tuned across the Brillouin zone, can be trivial (left, winding number 0), or topological (right, winding number 1). If, as in the example shown, none of $|v|$, $|w_x|$, and $|w_y|$ is bigger than sum of the other two, for some value of k_y, we will have the trivial, for others, the topological case. We then must have an intermediate value of k_y where the gap closes: a node.

sponding curves in the $d_x - d_y$ plane, as illustrated in Fig. 11.3, are circles of radius w_x, whose center is at $(v + w_y \cos k_y, w_y \sin k_y)$. Thus, as we tune k_y, the center of the circle is taken on a circle of radius w_y around $(v,0)$. If, as in the example shown, none of $|v|$, $|w_x|$, and $|w_y|$ is bigger than sum of the other two, for some value of k_y, we will have the trivial, for others, the topological case. We then must have two values of (k_y,k_x) where the gap closes: the nodes. We have

$$\begin{aligned} w_x < v - w_y : &\qquad \text{Trivial} \\ v - w_y < w_x < v + w_y : &\qquad \text{Topological semimetal} \\ v + w_y < w_x : &\qquad \text{Weak topological.} \end{aligned}$$

See Exercise 11.8.

In the topological semimetal case we have isolated points in the Brillouin zone where the gap closes. This is all quite natural when describing the model as a set of 1-dimensional chiral symmetric topological insulators, but in the full 2D model, it can appear strange at first sight. We need to investigate these gap closing points further.

11.2.1 Gap closing points

In the topological semimetal phase of a two-band two-dimensional model, the bulk is not fully gapped: the gap closes at isolated points in the Brillouin zone, the so-called nodes k. The nodes are the solutions of the equations,

$$d_x(k_x,k_y) = 0; \qquad \text{and} \qquad d_y(k_x,k_y) = 0. \tag{11.6}$$

These are two equations for two variables k_x and k_y, so we expect only isolated, point-like solutions, if any.

Continuously varying the parameters, each isolated pointlike node will move continuously along a path in the Brillouin zone. For our specific model of coupled SSH chains, we can find these paths. The gap closing requirements read

$$-v = w_x \cos K_x + w_y \cos K_y; \qquad w_x \sin K_x = -w_y \sin K_y, \tag{11.7}$$

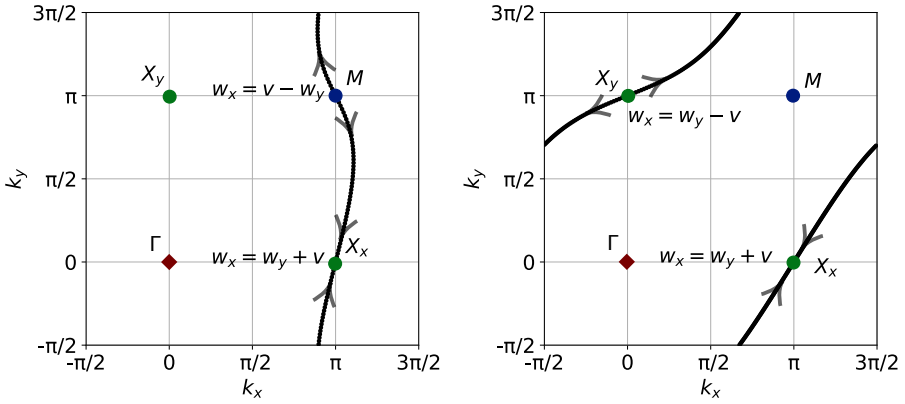

Figure 11.4: Paths of the nodes in the Brillouin zone. Left: $v = 1., w_y = 1/3$, tune w_x. Right: $v = 1., w_y = 5/3$, tune w_x.

and can be solved as

$$w_x = \sqrt{(v + w_y \cos K_y)^2 + w_y^2 \sin^2 K_y}; \tag{11.8}$$

$$K_x = \text{atan}_2(-w_y \sin K_y, -v - w_y \cos K_y), \tag{11.9}$$

using the atan_2 function, which returns $\phi \in (-\pi, \pi]$, if supplied with arguments $a \sin\phi$, $a\cos\phi$ for any $a > 0$.

Using a parameter, e.g., w_x, to tune the system across a broadened topological phase transition, we find that nodes are first born pairwise, then driven in opposite directions in the Brillouin zone, then annihilate pairwise. Examples with $v = 1$, $w_y = 1/3$, and $v = 1$, $w_y = 5/3$, are shown in Fig. 11.4. In our two-dimensional model this follows from inversion symmetry: nodes must come in inversion symmetric pairs of $(K_x, K_y) \leftrightarrow (-K_x, -K_y)$, and

$$\text{If} \quad v > w_y: \qquad v - w_y \le w_x \le v + w_y; \qquad M \to X_x; \tag{11.10}$$

$$\text{If} \quad v < w_y: \qquad w_y - v \le w_x \le v + w_y; \qquad X_y \to X_x. \tag{11.11}$$

However, even if inversion symmetry is broken, nodes can only be born and annihilated pairwise. As we show next, this has a deeper, topological reason.

11.3 Topological Charge of Nodes

The nodes in the topological semimetal, i.e., the isolated pointlike gap closing points, carry a topological charge, and are hence topologically protected. We show this first for the two-band model, and then generalize.

11.3.1 Two-band Model: Charge is Winding of d Around Node

Since our two-dimensional semimetal is a two-band model, we can gain more insight into the nature of the nodes by taking a look at the $\vec{d}$ field, defined by $\hat{H}(k_x,k_y) = \vec{d}(k)\hat{\sigma}$. An example for $w_x = w_y = v = 1$ is shown in Fig. 11.5. Here, the two nodes are at $K_x = -K_y = \pm 2\pi/3$, and you can see that the d field winds around these points. We can put the calculation into a convenient form using

$$\mathbf{d}(\mathbf{k}) = d(k)\cos\phi(\mathbf{k})\tilde{\mathbf{x}} + d(k)\sin\phi(\mathbf{k})\tilde{\mathbf{y}}, \tag{11.12}$$

where $\tilde{\mathbf{x}}$ and $\tilde{\mathbf{y}}$ are unit vectors along the two axes.

Put a discrete lattice on the Brillouin zone. We assign numbers to the vertices, edges, and plaquettes of the lattice, as

$$\text{vertex } k_a : \phi(k_a) = \text{atan}_2(d_x(k_a), d_y(k_a)); \tag{11.13a}$$

$$\text{edge } k_a \to k_b : \quad \phi_{ab} = \arg\left(e^{i\phi(k_b) - i\phi(k_a)}\right); \tag{11.13b}$$

$$\text{plaquette } p : \quad Q_p = \frac{1}{2\pi}\left(\phi_{ab} + \phi_{bc} + \phi_{cd} + \phi_{da}\right), \tag{11.13c}$$

where the plaquette p has boundary $a \to b \to c \to d \to a$. The quantity $Q_p \in \mathbb{Z}$ counts the vorticity of the vector field d in the plaquette p.

A discrete Stokes theorem, for a disk $\mathscr{S}$ composed of plaquettes, reads

$$\sum_{(ab)\in\partial\mathscr{S}} \phi_{ab} = 2\pi \sum_{p\in\mathscr{S}} Q_p. \tag{11.14}$$

It can be proven by just rearranging the sums on the right-hand-side. The discrete Stokes theorem has two important consequences.

Jump in weak topoogical invariant happens when $k_y = K_y$.

Total topological charge has to be 0. This is because the quantities we defined in the Brillouin zone are all periodic.

Continuum Limit

We can put this in a more convenient form by introducing a vector field $\mathbf{A}(k_x,k_y)$, which is in some sense a gradient of $\phi(k_x,k_y)$. This is easiest to define using square plaquettes (can be done for plaquettes of arbitrary shape), with corners

$$k_a = (k_x - \delta_k/2, k_y - \delta_k/2); \qquad k_b = (k_x + \delta_k/2, k_y - \delta_k/2);$$
$$k_c = (k_x + \delta_k/2, k_y + \delta_k/2); \qquad k_d = (k_x - \delta_k/2, k_y + \delta_k/2).$$

The definition reads,

$$\mathbf{A}(k_x,k_y) = \frac{\phi_{ab} + \phi_{dc}}{2\delta_k}\tilde{\mathbf{x}} + \frac{\phi_{ad} + \phi_{bc}}{2\delta_k}\tilde{\mathbf{y}}. \tag{11.15}$$

The vorticity Q_p corresponds to the flux of the curl of the vector field $\mathbf{A}$ on the plaquette p.

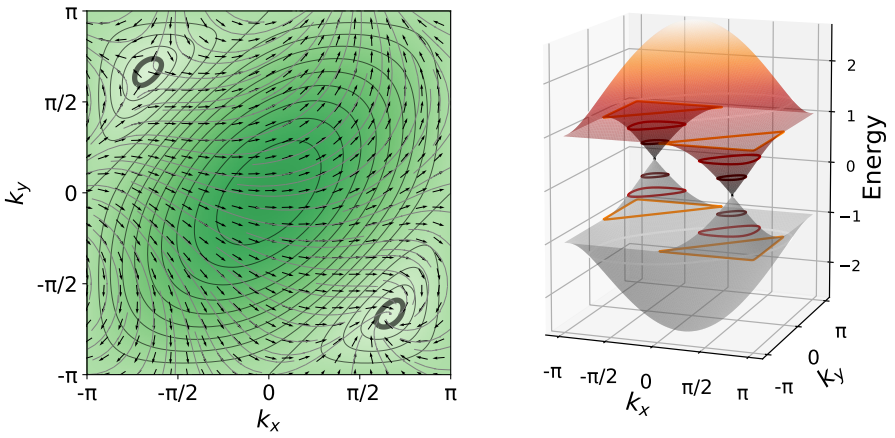

Figure 11.5: Brillouin zone, with d vectors. $v = w_x = w_y = 1$.

The Stokes theorem above reads, for a disk $\mathscr{S}$ with boundary $\partial\mathscr{S}$,

$$\oint_{\partial\mathscr{S}} \mathbf{A} ds = \int_{\mathscr{S}} \nabla \times \mathbf{A} d^2 S \tag{11.16}$$

Since $\mathbf{A}$ is a gradient, its curl vanishes, except at points where it is not well defined.

Linearizing Around the Nodes: Charge is Determinant

Two-band case, linearized around a Weyl node K, we have, using the small distance $\mathbf{p} = \mathbf{k} - \mathbf{K}$,

$$\hat{H}_{\mathrm{C2D}} \approx \begin{pmatrix} p_x & p_y \end{pmatrix} \underbrace{\begin{pmatrix} v_{xx} & v_{xy} \\ v_{yx} & v_{yy} \end{pmatrix}}_{\underline{\underline{v}}} \begin{pmatrix} \hat{\sigma}_x \\ \hat{\sigma}_y \end{pmatrix}; \tag{11.17}$$

$$v_{ax} = -w_a \sin K_a; \qquad v_{ay} = w_a \cos K_a \quad \text{for } a \in \{x, y\}. \tag{11.18}$$

For the Hamiltonian to be Hermitian, the matrix $\underline{\underline{v}}$ of coefficients must be real.

We can map how the vector field $d(p)$ winds around the node by solving the linearized equations for $d_x = 0$ and $d_y = 0$:

$$d_x = 0: \quad p_y = -\frac{v_{xx}}{v_{yx}} p_x; \qquad d_y = 0: \quad p_y = -\frac{v_{xy}}{v_{yy}} p_x. \tag{11.19}$$

The winding number is then found to be

$$\nu = \operatorname{sign} \det \underline{\underline{v}}. \tag{11.20}$$

11.3.2 More bands: Charge is winding of det h around node

For topological semimetals with more than 2 bands, we need to generalize the formulas above that relied explicitly on the vector **d**. Before we do that, we remark that we could still use the 2-band formulas in the vicinity of each node if only two energy levels are intersecting there.

To build more general formulas, we use chiral symmetry of the Hamiltonian. For the matrix of the bulk momentum-space Hamiltonian this reads,

$$H(k_x,k_y) = \begin{pmatrix} 0 & h(k_x,k_y) \\ h^\dagger(k_x,k_y) & 0 \end{pmatrix}. \tag{11.21}$$

We can apply the same formalism as before, but instead of the phase of the vector **d**, use the phase of the complex number $\det h(k)$.

$$\text{vertex } k_a: \quad \det h(k_a); \tag{11.22a}$$

$$\text{edge } k_a \to k_b: \quad \phi_{ab} = \arg\left(\frac{\det h(k_b)}{\det h(k_a)}\right); \tag{11.22b}$$

$$\text{plaquette } p: \quad Q_p = \frac{1}{2\pi}\left(\phi_{ab}+\phi_{bc}+\phi_{cd}+\phi_{da}\right), \tag{11.22c}$$

11.4 Fermi Arcs – Edge States in Part of the Brillouin Zone

Topological semimetals can have edge states, which occupy only a part of the "edge Brilouin zone".

This is best illustrated through a concrete example, obtained by tuning our 2D model from trivial to weak topological insulator, and plotting dispersions relations of a system with edges, as in Fig. 11.6. Notice first how bulk nodes appear, separate, and then meet and annihilate again. Notice also that there is a line of edge states for both edge orientations, which connects the bulk nodes. Focusing on the edge along y (upper row), the we can demote momentum k_y to a parameter, and the topological semimetal is seen as a set of 1D chiral symmetric chains, each with its label k_y. Some, of these chains are topological, some of them trivial. For the k_y's of topological chains, we have to have edge states.

From this example we can understand that a flat line of edge states that covers only part of the edge Brillouin Zone, terminated by the bulk nodes, is a generic feature of topological semimetals.

There are some remarks to be made regarding the robustness of these edge states protected by chiral symmetry. At the edge, the natural boundary condition might still respect chiral symmetry in the sense of only having nearest-neighbour coupling, but the integrity of unit cells is often not maintained. This means that these edge states are not as robust as those of strong topological insulators.

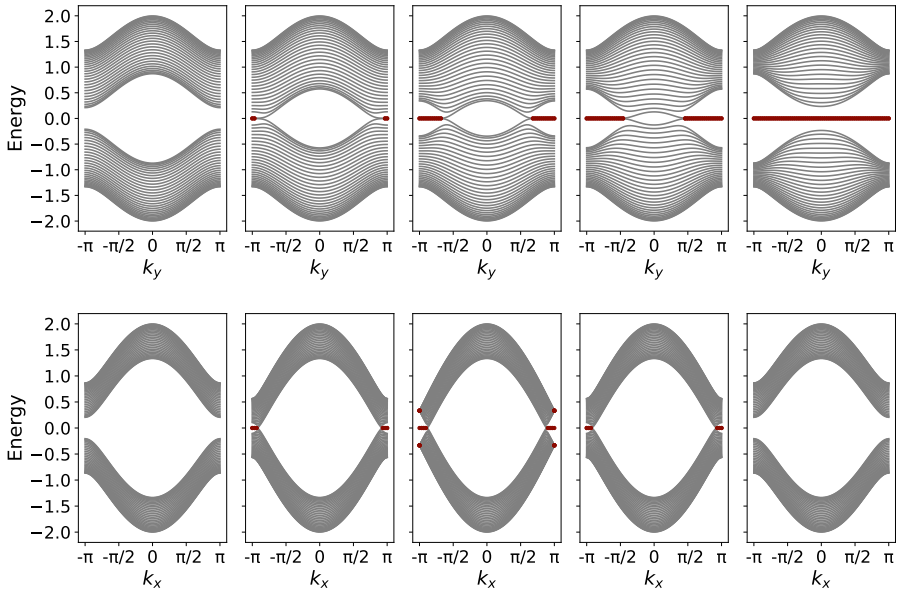

Figure 11.6: Transition from trivial insulator to a weak topological insulator, obtained by tuning w_x. Interchain coupling is $w_y = 1/3$, and parameters are set so that $w_x + w_y + v = 2$. From left to right, $v, w_x = (1.1, 0.566), (0.95, 0.716), (5/6, 5/6), (0.716, 0.95), (0.566, 1.1)$. Top row: cut along y. Bottom row: cut along x. Large (red) dots indicate edge states (whose wavefunction has over 40% weight within the first 6 unit cells of the total of 30 unit cells)

11.5 Three-dimensional Weak Topological Insulators: Coupling QWZ Layers

We now go one dimension higher, and obtain a toy model for a three-dimensional (3D) weak topological insulator by coupling layers of a two-dimensional topological insulator. We will see the same steps as in the chiral symmetric 2-dimensional case above: weak topological phases can be defined, the transition from trivial to weak topological is broadened, and the intermediate case is a topological semimetal. The important difference is that for the 3D case, we don't need to rely on any symmetry, and therefore the consequences will be more robust.

We define a 3-dimensional model Hamiltonian by coupling layers of the QWZ model. The bulk momentum-space Hamiltonian reads,

$$\hat{H}_{\text{Weyl}}(k) = \sin k_x \hat{\sigma}_x + \sin k_y \hat{\sigma}_y + (u + w\cos k_z + \cos k_x + \cos k_y)\,\hat{\sigma}_z. \tag{11.23}$$

This model reduces to the one cited in Vishwanath by setting $w = 1$. We do not have chiral symmetry here, neither time-reversal symmetry, but we do have inversion symmetry and mirror symmetry along z:

$$\text{Inversion symmetry} : \quad \hat{\sigma}_z \hat{H}_{\text{Weyl}}(k)\hat{\sigma}_z = \hat{H}_{\text{Weyl}}(-k); \tag{11.24}$$

$$\text{Mirror symmetry} : \quad \hat{H}_{\text{Weyl}}(k_x,k_y,k_z) = \hat{H}_{\text{Weyl}}(k_x,k_y,-k_z). \tag{11.25}$$

Neither inversion symmetry nor mirror symmetry play any important role here, they can be broken. For example, we could break inversion symmetry with $w'\sin(k_z)\hat{\sigma}_x + w'\cos(k_z)\hat{\sigma}_y$.

This model is a weak Chern insulator. The set of bulk topological invariants are the Chern numbers Q_x, Q_y, Q_z of slices of the system perpendicular to x, y, z. For example, Q_z is obtained by 1) demoting k_z to parameter, 2) setting it to any fixed value, e.g., $k_z = 0$, and 3) calculating the Chern number of $\hat{H}_{\text{Weyl}}(k_x, k_y, 0)$.

A weak Chern insulator has edge states on clean edges, as predicted by the weak invariants. These are not (flat bands of) 0-energy states, as in case of the 2-dimensional chiral weak topological insulator, but rather propagating states.

11.6 Transition from Trivial to Weak Topological Broadened: Topological Semimetals

For the model Hamiltonian composed of a stack of QWZ layers, eq. (11.23), we can tune the transition from trivial to weak topological insulator via the onsite Zeeman parameter u.

If the layers are not coupled, $w = 0$, the transitions happen instantaneously. We transition from trivial ($u < -2$) to weak Chern insulator with $Q = +1$ ($-2 < u < 0$) at $u = -2$, to another weak Chern insulator with $Q = -1$ ($0 < u < 2$) at $u = 0$, to trivial phase again ($u > 2$) at $u = 2$. At the transition points, the bulk gap closes along lines spanning the whole Brillouin zone.

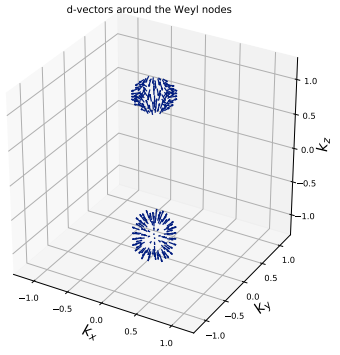

Figure 11.7: Brillouin zone, with d vectors. $u = -2$, $v = 0.05$.

If the layers are coupled, the transitions broaden and we have an intermediate topological semimetal phase, much in the same way as in the lower dimensional case. We can treat the momentum k_z as a parameter. The three-dimensional model is then described by a torus that is moved periodically in d-space, as the parameter k_z is tuned from $-\pi$ to π. There will be a broad parameter range where during one cycle at two values of k_z this surface will contain the origin. At these values of k_z, the bulk gap closes at a nodal point, some specific k_x, k_y, k_z. The two nodal points will have some sort of chirality that is opposite, because of opposite velocity of the surface at the two values of k_z points. More on this later.

In the presence of coupling, each gap closing along the lines at a single u value is turned into the trajectory of the node, at a finite range of u.

$u < -2 - w$:	Trivial;
$-2 - w < u < -2 + w$:	Semimetal, $(0,0,0 \to \pm\pi)$;
$-2 + w < u < -w$:	Weak Chern;
$-w < u < w$:	Semimetal, $(0,\pi,0 \to \pm\pi)$ and $(\pi,0,0 \to \pm\pi)$;
$w < u < 2 - w$:	Weak Chern;
$2 - w < u < 2 + w$:	Semimetal, $(\pi,\pi,0 \to \pm\pi)$;
$2 + w < u$:	Trivial.

Weyl nodes are confined to four columns in the Brillouin zone, $k_x = 0, \pi$ and $k_y = 0, \pi$, every Weyl node at k comes with its inversion symmetric partner at $-k$. Breaking inversion symmetry turns the columns into helical columns.

11.7 Topologically Protected Nodes: Gap Closing Points

11.7.1 Two-band Model: Nodes are Sources or Sinks of $\tilde{\mathbf{d}}$.

We can gain more insight into the nature of the nodes by taking a look at the $\vec{d}$ field. We can put the calculation into a convenient form using

$$\hat{H}_{\text{Weyl}}(k) = d_0(k)\sigma_0 + \mathbf{d}(k)\hat{\boldsymbol{\sigma}} = E_-(k)\,|u_-(k)\rangle\,\langle u_-(k)| + E_+(k)\,|u_+(k)\rangle\,\langle u_+(k)|\,, \tag{11.26}$$

with $E_-(k) < 0$, $E_+(k) > 0$, and $\langle u_+(k)\,|\,u_-(k)\rangle = 0$ for every momentum k. In our model, $d_0(k) = 0$, and hence, $E_-(k) = -E_+(k)$, which is important because it puts the nodes at the Fermi surface for half filling.

We will use a simplified notation:

$$\tilde{\mathbf{d}}(k) = \mathbf{d}(k)/\,|\mathbf{d}(k)|\,; \tag{11.27}$$

$$k = k_a: \quad \tilde{\mathbf{d}}_a = \tilde{\mathbf{d}}(k_a); \quad |a\rangle = |u_-(k_a)\rangle\,. \tag{11.28}$$

The main idea of the calculation is best appreciated by starting in the continuum. In a volume $\mathscr{V}$ with surface $\mathscr{S} = \partial\mathscr{V}$, we can find the total number of sources/sinks of the vector field $\mathbf{d}(k)$, by calculating the solid angle the vector field $\tilde{\mathbf{d}}$ sweeps over as we scan over the surface.

For the discretization we will need a geometrical formula for the solid angle. We could do this using

$$\frac{1}{2}\Omega_{abc} = \tan^{-1}\left(\frac{\left(\tilde{\mathbf{d}}_a \times \tilde{\mathbf{d}}_b\right)\tilde{\mathbf{d}}_c}{1 + \tilde{\mathbf{d}}_a\tilde{\mathbf{d}}_b + \tilde{\mathbf{d}}_a\tilde{\mathbf{d}}_c + \tilde{\mathbf{d}}_b\tilde{\mathbf{d}}_c}\right), \tag{11.29}$$

but this is a bit cumbersome, and it would restrict us to triangular plaquettes. We can do something more efficient, by using the knowledge obtained previously that the solid angle corresponds to the discrete Berry phase,

$$\frac{1}{2}\Omega_{abc} = F_{abc} = \arg\left(\langle a\,|\,b\rangle\,\langle b\,|\,c\rangle\,\langle c\,|\,a\rangle\right), \tag{11.30}$$

which is valid for plaquettes with any number of nodes on the boundary.

The discretization is obtained as

$$\text{node } a: \quad |a\rangle\,; \tag{11.31}$$

$$\text{edge } a \to b: \quad \langle a\,|\,b\rangle\,; \tag{11.32}$$

$$\text{plaquette } p: \quad F_p = \arg \prod_{(ab)\in\partial p} \langle a\,|\,b\rangle\,; \tag{11.33}$$

$$\text{volume element } v: \quad Q_v = \frac{1}{2\pi}\sum_{p\in\partial v} F_p. \tag{11.34}$$

We have to pay attention to the proper orientations of the boundaries: for plaquettes these are counterclockwise, for volume elements, the plaquettes should all be defined

with normal oriented out from the middle of the volume element. We can plug in the arguments from the section on the Chern number, and obtain that the quantities Q_p are integers, and they detect the nodes.

A discrete Gauss theorem, for a volume $\mathscr{V}$ composed of volume elements,

$$\sum_{(p)\in\partial\mathscr{V}} F_{ab} = \sum_{v\in\mathscr{V}} Q_v. \tag{11.35}$$

This has two important consequences.

Jump in weak topoogical invariant happens when $k_y = K_y$.

Total topological charge has to be 0. This is because the quantities we defined in the Brillouin zone are all periodic.

Continuum Limit

We can put this in a more convenient form by introducing a vector field $\mathbf{B}(k_x,k_y)$, the Berry curvature. This is easiest to define using cubic volume elements (possible for volume elements of arbitrary shape), with corners

$$\begin{aligned}
k_a &= \left(k_x-\frac{\delta_k}{2},k_y-\frac{\delta_k}{2},k_z-\frac{\delta_k}{2}\right); & k_b &= \left(k_x+\frac{\delta_k}{2},k_y-\frac{\delta_k}{2},k_z-\frac{\delta_k}{2}\right);\\
k_c &= \left(k_x+\frac{\delta_k}{2},k_y+\frac{\delta_k}{2},k_z-\frac{\delta_k}{2}\right); & k_d &= \left(k_x-\frac{\delta_k}{2},k_y+\frac{\delta_k}{2},k_z-\frac{\delta_k}{2}\right);\\
k_e &= \left(k_x-\frac{\delta_k}{2},k_y-\frac{\delta_k}{2},k_z+\frac{\delta_k}{2}\right); & k_f &= \left(k_x+\frac{\delta_k}{2},k_y-\frac{\delta_k}{2},k_z+\frac{\delta_k}{2}\right);\\
k_g &= \left(k_x+\frac{\delta_k}{2},k_y+\frac{\delta_k}{2},k_z+\frac{\delta_k}{2}\right); & k_h &= \left(k_x-\frac{\delta_k}{2},k_y+\frac{\delta_k}{2},k_z+\frac{\delta_k}{2}\right).
\end{aligned}$$

The components of the field B are defined using the Chern numbers of the appropriate plaquettes, calculated so the normals are always along the positive direction, i.e.,

$$\mathbf{B}(k_x,k_y,k_z) = \frac{F_{adhe}+F_{bcgf}}{2\delta_k^2}\,\tilde{\mathbf{x}} + \frac{F_{aefb}+F_{dhgc}}{2\delta_k^2}\,\tilde{\mathbf{y}} + \frac{F_{abcd}+F_{efgh}}{2\delta_k^2}\,\tilde{\mathbf{z}}.$$

It is easy to show that Q_v corresponds to the integral of the divergence of the vector field $\mathbf{B}$ on the volume element v.

The Gauss theorem above reads, for a volume element $\mathscr{V}$ with boundary $\partial\mathscr{V}$,

$$\oint_{\partial\mathscr{V}} \mathbf{B}(k)d^2k = \int_{\mathscr{V}} \text{div}\,\mathbf{B}(k)d^3k \tag{11.36}$$

Because of the connection between the Chern number and the solid angles,

$$\mathbf{B} = \text{curl}\,\tilde{\mathbf{d}}. \tag{11.37}$$

Since $\mathbf{B}$ is a curl, its divergence vanishes, except at points where it is not well defined.

Linearizing Around the Nodes: Charge is Determinant

Two-band case, linearized around a Weyl node K, we have, using the small distance $\mathbf{p} = \mathbf{k} - \mathbf{K}$,

$$\hat{H} \approx \begin{pmatrix} p_x & p_y & p_z \end{pmatrix} \begin{pmatrix} v_{xx} & v_{xy} & v_{xz} \\ v_{yx} & v_{yy} & v_{yz} \\ v_{zx} & v_{zy} & v_{zz} \end{pmatrix} \begin{pmatrix} \hat{\sigma}_x \\ \hat{\sigma}_y \\ \hat{\sigma}_z \end{pmatrix}; \tag{11.38}$$

In general, the matrix $\underline{\underline{v}}$ of coefficients is real.

We can map how the vector field $d(p)$ winds around the node, ... The charge of the node is then found to be

$$\nu = \operatorname{sign} \det \underline{\underline{v}}. \tag{11.39}$$

11.7.2 General, multiband case

The formulas obtained through linearization also apply to the multiband case. In the vicinity of each node, only two energy levels are interesting anyway, we can use the restriction of the Hamiltonian to those levels.

For more general formulas, we can plug in the formulas for Chern number of multiband systems.

$$\hat{H}(k_a) = \sum_{m=1}^{N_F} E_m(k_a) \left|a_m\right\rangle \left\langle a_m\right| + \sum_{m=N_F+1}^{N_{\text{tot}}} E_m(k_a) \left|a_m\right\rangle \left\langle a_m\right|; \tag{11.40}$$

We are interested in the nodes between the N_Fth and the (N_F+1)th energy states. This is crucial if for all k, we have $m \leq N_F \Rightarrow E_m(k) \leq 0$ and $m > N_F \Rightarrow E_m(k) \geq 0$.

The derivations for the two-band case remain valid, with the replacement $\langle a \,|\, b \rangle \to \det M^{(ab)}$. Put a discrete three-dimensional lattice on the Brillouin zone. We assign objects to the vertices, edges, plaquettes, and cubes of the lattice,

$$\begin{aligned} \text{vertex } a: &\quad \{|a_1\rangle, |a_2\rangle, \ldots, |a_{N_F}\rangle\}; \\ \text{edge } a \to b: &\quad \det M^{(ab)}, \text{ with } M^{(ab)}_{mn} = \langle a_m \,|\, b_n \rangle; \\ \text{plaquette } p: &\quad F_p = \arg \prod_{(ab) \in \partial p} \det M^{(ab)} \\ \text{volume element } v: &\quad Q_v = \frac{1}{2\pi} \sum_{p \in \partial v} F_p. \end{aligned}$$

11.8 Fermi Arcs on Surface

The edge states exist only in parts of the Brillouin zone: those parts where the weak Chern number is nonzero. These are the Fermi arcs.

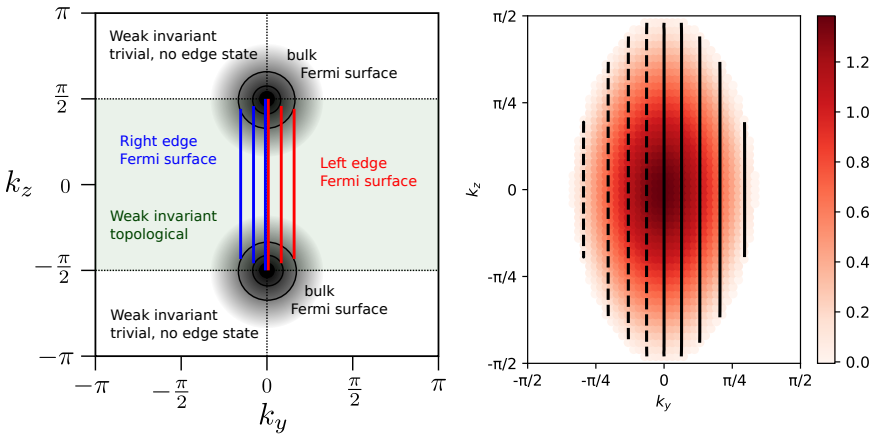

Figure 11.8: Edge states of a Weyl semimetal. Color: inverse of the localization length of edge state. Fermi arcs are equipotential lines, shown in thick lines, continuous for energy $E = 0$ and above, slashed for negative energy. Spacing between equienergy lines is 0.2

Problems

Nodes protected by extra symmetries

POSSIBLE EXERCISE: Even if chiral symmetry is broken, these other symmetries can stabilize the Weyl nodes. This is trivial in two-level systems, how does it work out in general?

Transition from weak topological

Discuss what happens to the two-dimensional chiral symmetric lattice model, as w_x is tuned from $w_x = 0$ to $w_x = 10$, if $v = 1$ and $w_y = 2$.

Answer: If we repeat the same process, but with topological chains, $v < w_y$, we have

$$\text{If} \quad w_x < w_y - v: \qquad \text{Weak topological;} \tag{11.41}$$

$$\text{If} \quad w_y - v < w_x < v + w_y: \qquad \text{Semimetal;} \tag{11.42}$$

$$\text{If} \quad v + w_y < w_x: \qquad \text{Weak topological.} \tag{11.43}$$

Paths of nodes when v is tuned

If v is tuned, show that, assuming $w_y < w_x$ without loss of generality,

$$w_x - w_y \le v \le w_x + w_y; \qquad X_y \to M \tag{11.44}$$

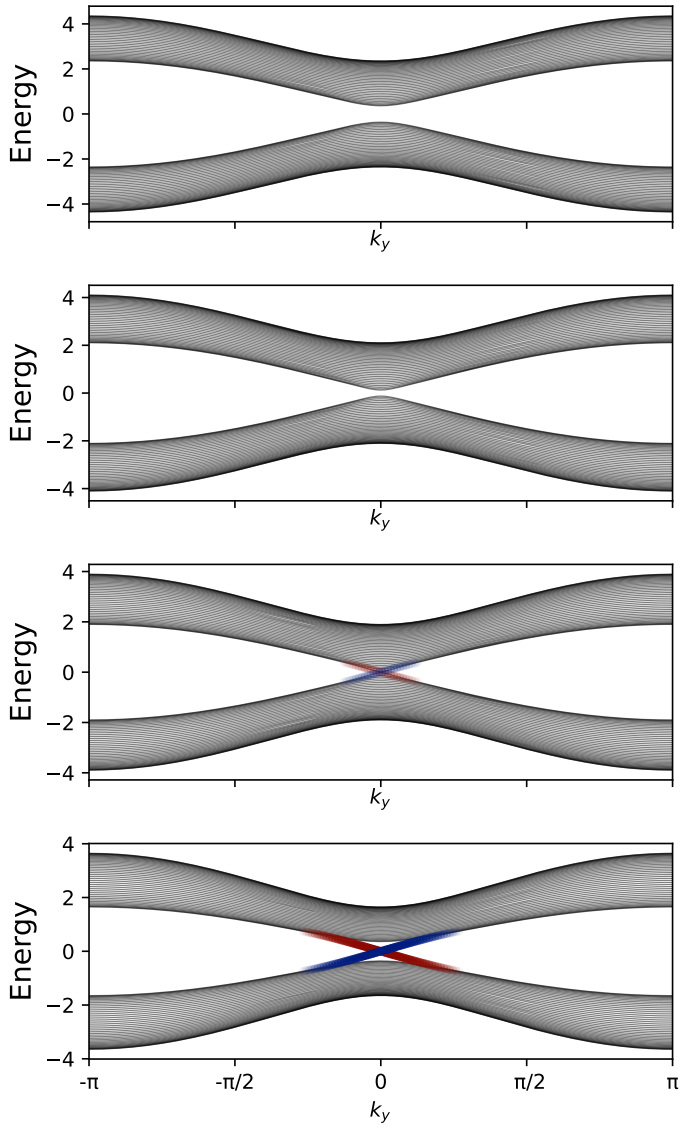

Figure 11.9: Edge states of a Weyl semimetal. Color: inverse of the localization length of edge state. Fermi arcs are equipotential lines, shown in thick lines, continuous for energy $E = 0$ and above, slashed for negative energy. Spacing between equienergy lines is 0.2